DOE/NV/03624--0842

Geant4 and MCNP6.2 modeling of fast-neutron detectors based on single-crystal chemical vapor deposition diamond

J. Andrew Green*[a], Amber L. Guckes[a], Robert Buckles[a], Derek Constantino[a], Joshua Friedman[a], Joseph Tabeling[b], Adam J. Wolverton[a]

[a]Nevada National Security Site, Nevada Operations, 2621 Losee Road, North Las Vegas, NV, USA 89030; [b]Applied Diamond, Inc., 3825 Lancaster Pike, Wilmington, DE USA 19805

ABSTRACT

Diamond photoconductive detectors have been shown to detect fast neutrons with high gamma insensitivity. Depending on the application and the incident neutron energy, there are many possible choices when considering how diamond elements may be sized, arranged, and instrumented. As part of our design effort, we are using Geant4 and MCNP6.2 to simulate the effects of fast neutrons impinging on diamond detectors ranging in thickness from a few microns to a few hundred microns that are 4 mm on a side with intervening materials and other physical parameters. The models may be used to compare diamond detector measurements with incident neutrons ranging from ~1 to 14.1 MeV to better understand the nuclear and atomic physics effects contributing to an electronic signal. We are investigating pulse height, signal-to-noise ratio, and timing characteristics of prototype single-crystal chemical vapor deposition diamond detectors.

Keywords: Neutron detection, gamma insensitivity, diamond, avalanche, Geant4, MCNP6.2

1. INTRODUCTION

The dimensions being considered are 4 mm on a side and multiple thicknesses in the range of 5 to 500 microns. We are interested in using diamond-based detectors to augment the detection of neutrons created in a dense plasma focus (DPF) pinch. These are nominally 14.1 MeV neutrons created by deuterium-tritium (D-T) fusion. The goal of these detectors is to measure the position of the neutron pinch as well as the neutron intensity close to the DPF source. These detectors are part of the larger effort of the Stockpile Stewardship program to measure the properties of the nuclear materials currently in use, which will feed the highly complex simulations required to improve predictive capabilities.

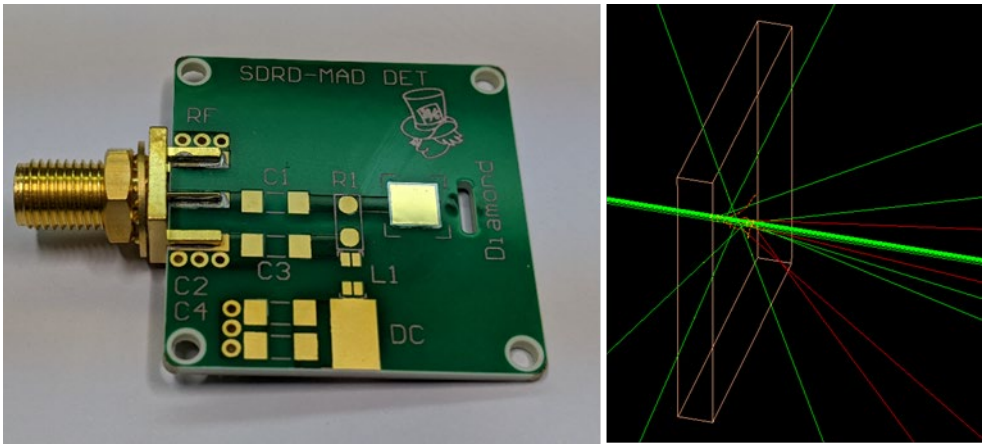

Figure 1. The board used to make the first measurements of the 10- and 5-micron diamond detectors at various bias voltages. The detector was illuminated by a small D-T neutron generator. This was done in the Source Range Laboratory at the Nevada National Security Site (NNSS) facility in North Las Vegas, NV. The figure on the right shows an example of several simulated neutron events within the diamond. The neutron beam enters from the left with neutrons (green) and electrons (red) exiting. The remaining charge displaced (the ~1-micron ion tracks are too small on this scale) is on the order of 1E5 electrons per neutron interaction. This charge is swept by the bias and detected by the anode on the board.

*greenja@nv.doe.gov; phone 1 702 295-2688; nnss.gov

The detector simulation work computes the effects of neutrons and gammas/x-rays impinging on a thin diamond target, the purpose of which is to understand how signal is generated and how to improve signal-to-noise ratio. We will show a number of interesting results that ultimately help understand how charge is liberated in the body of the diamond detector. This leads to predicting the magnitude and timing of the detected signal. Various high-voltage values are applied across the thickness, and the charge is read out with an anode at the base of the diamond. Shown in Figure 1 is the board with a mounted 4 mm × 4 mm × 10 micron diamond. The measurements, which will be reported in an upcoming document, were also accompanied with these Monte Carlo predictions of the energy deposition (E_{dep}) in the diamond.

2. BACKGROUND

2.1 Performance of electronic grade diamond as a radiation detector

Electronic grade diamond continues to be exploited as a solid-state radiation detector due to several of its intrinsic characteristics.[1,2,3] Diamond has a large bandgap of 5.5 eV, which categorizes it as an insulator.[4] Thus, only incident radiation can knock loose charge in the detector—not ambient light or thermal activity. As compared to other solid-state technologies that must be cooled to reduce thermal noise, this manifests as improved signal-to-noise ratio during the performance of measurements. Due to high electron and hole mobilities, diamond also has a very fast time response on the order of 1 nanosecond[5] or less, depending on thickness. This is very attractive for current mode measurements. It is also very radiation hard, requiring a very large flux of radiation over a long period of time before the diamond signal loses linearity.[6]

Although diamond detectors have been and continue to be used for the measurement of x-rays, gamma rays, and charged particles, the low effective atomic number and density of diamond make it a worthwhile neutron detector. Diamond detectors have been fielded as neutron diagnostics on experiments such as at the National Ignition Facility and Z machine.[7,8,9]

2.2 Diamond detectors for neutron diagnosed subcritical experiments

Leveraging the performance of diamond detectors on the aforementioned experiments, a 500 μm thick single-crystal chemical vapor deposition (scCVD) diamond detector has been fielded as part of the Neutron Diagnosed Subcritical Experiments (NDSE) static campaign to measure the neutron source term as a function of time.[10] The source used in this experiment is a D-T DPF that creates ~2E12 14.1 MeV neutrons into a solid angle of 4-pi steradians in ~75 ns.[10] Understanding the neutron interactions in the diamond and the resultant electron-hole transport is crucial in interpreting the measured data and is informative for optimizing the design of future diamond detectors to be fielded on the NDSE series of both static and dynamic campaigns. Monte Carlo simulations provide a valuable predictive capability to inform the performance of both the current and future diamond detector designs.

3. METHODOLOGY

3.1 Geant4 simulations

The scCVD diamond detector fielded for the NNSS NDSE static campaign was modeled in Geant4 version 4.10.03 as a simple 4 × 4 × 0.5 mm^3 rectangular block as shown in Figures 1 and 2. The material properties of the diamond detector model was set to natural carbon abundance (98.93% ^{12}C and 1.07% ^{13}C) with a density of 3.51 g/cm^3.

Although we refer to the diamond as single crystal in this work, our Geant4 application models it as aggregate material of the given density and relative abundance of isotopes. This is completely adequate to encompass the nuclear physics of neutrons impinging on a target of given material and subsequent shower energy losses of secondaries. Assumptions about its crystalline properties are only used in signal and electronics calculations that require the Geant4-based simulation as input. For instance, the assumption of linear transport of electrons and holes and the effect of associated bias fields, detector capacitance, and so forth are modelled "downstream" from the nuclear physics. In general, the Geant4 library does have the capability to handle a full end-to-end simulation, but we instead use other well-understood techniques implemented in Matlab®, COMSOL®, and others.

The neutron cross sections are from the ENDF VIII (2018) database. The physics reference list, Fritiof-Bertini with Neutron High-Precision, known as FTFP_BERT_HP, is the one recommended for use with neutron energies below 20 MeV.[13] This physics reference list covers a wide variety of models that are assigned to associated particles and energy ranges. This physics package covers the range of neutron physics in our range of interest as well as it does for much

higher energies. Up to this point, we have chosen to use this predefined package rather than select or modify a custom package or model. For neutrons, the processes modeled include transport, elastic and inelastic nucleon-nucleus, capture, and nucleus de-excitation. The electromagnetic processes and cross sections and energy loss are applied for secondary charged particles, such as electrons, positrons, and ions. As a point for later study FTFP_BERT_HP uses the empirical "natural" cross sections of neutrons on carbon instead of those of the individual isotopes of ^{12}C and ^{13}C. This fact is reported at the beginning of our jobs in which this package is turned on.

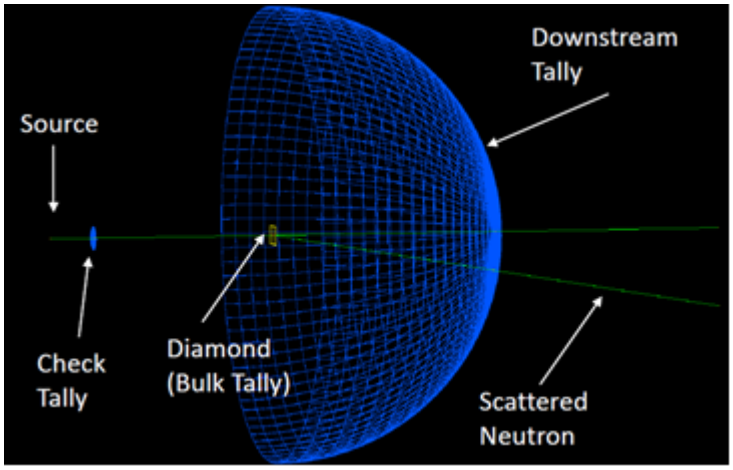

Figure 2. Three-dimensional representation of Geant4 diamond detector model. The beam particles move from left to right in the diagram. The "tallies" are well-defined planes (or shells) where information about all of the particles passing through are sampled and recorded.

3.1.1 Geant4 user configuration

Geant4 is a general-purpose library of classes. It requires that the user create her own C++ application using the library and following certain protocols for the simulation of events to run correctly. Needless to say, the user should be familiar with C++ and object-oriented programming with classes; however, mastery is not necessary. Typically, the application writer will use one of the many working examples that come with the Geant4 download as a template for building the application, so it is rare that one would write the application from scratch. It is also typical that the writer of the application is responsible for the analysis of the resulting simulation data. The minimum items for which the user is responsible are listed below:

1. Selection of the physics package, a custom combination of physics models, or a set of model(s) of the user's design (FTFP_BERT_HP)
2. Definition of the source distributions of particles that start the simulation (neutrons, gammas, up to about 14.5 MeV)
3. Definition of material properties and detector geometry (see above description)
4. Output of the simulation in the form of any data that the user desires such as screen printout, visualization, text files, histograms, ROOT trees, or anything to which the user has access
5. The main program and instantiation of required components (classes) for a simulation to occur
6. Compilation of the application to create the executable

All components are registered to the run manager, which handles the "logistics" of generating and tracking the particles, and inserting user custom codes in the right places in execution. In the general sense, we have already covered items 1 through 3, and we will subsequently cover 4. Items 5 and 6 and the specific protocols and classes to use are outside the scope of this document.

3.1.2 Output

In our case, the output data are in the form of three things: screen/visualization, histograms, and ROOT[14] ntuples. Figure 2 shows an example screen capture of the visualization, which can be rotated, zoomed, and so forth to display a few

events or to debug the geometry. The screen output (not shown) simply gives status of the simulation as it is being initialized and running; the user is free to add output or adjust verbosity of the text. For production runs of more than a few events, the batch mode is used that suppresses the graphics, but the text output generally remains and is redirected to a file for later reference.

The histograms (Figure 3) monitor the beam energy, beam direction, and other functions that inform the essential validity of the simulation.

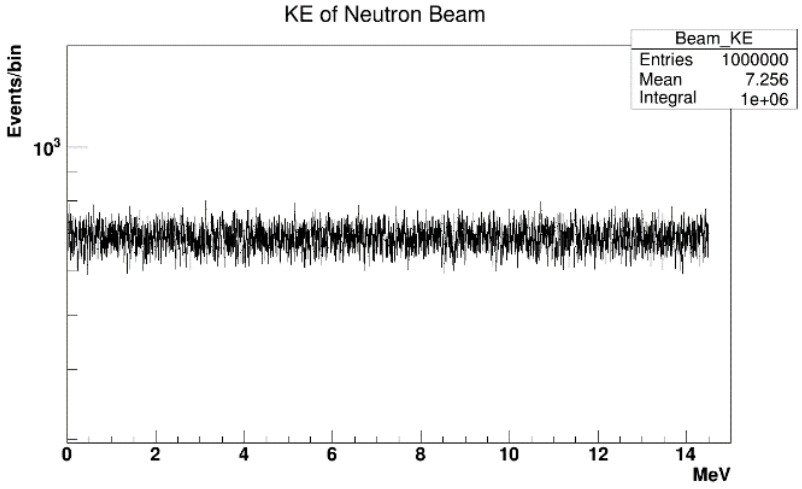

Figure 3. For the case of neutron events, we generated 1E6–1E9 neutrons across a uniform energy spectrum from 10 KeV to 14.5 MeV. The runs to date include gammas and neutrons of either 14.1 MeV or a uniform spectrum in energy. The uniform beam spectrum provides a basis for computing "functions" of beam energy such as the energy deposited per beam event as described later.

Table 1. The list of variables saved for the each particle track in these Geant4 diamond simulations.

Ntuple variable	Explanation
Event number	This allows multiple tracks in the event to be tied together.
Track ID number	A unique integer for each track in the event is assigned. This is used to accumulate information about a track if it appears in more than one place in the event. The beam particle is always track ID #1.
Particle ID	Identifies the particle type, and charge, and other properties as applicable.
Atomic number, atomic mass	If one of the particles is an ion or an alpha particle, then these values are nonzero.
Number of interactions for this track	How many times this particle had a discrete physics interaction (not including continuous energy loss below threshold for creation of secondaries).
Time	The time in ns at which the track either comes to rest or leaves the volume is provided by Geant4 tracking. Time zero for any given event is the start of that event's the beam particle.
Kinetic energy, initial and final	This is the relativistic kinetic energy of the particle at the beginning of the track and at the end.

Ntuple variable	Explanation
Energy deposited by the track	This is the energy loss directly attributed to the particle. For instance, gammas and neutrons have almost no energy loss attributed to them. However, their secondary (child) electrons and ions are assigned an energy loss per their individual energy, mass, and charge and dE/dx. For a given event, energy deposition is not double counted, which means that a simple sum of the energy depositions will yield the energy deposition (E_{dep}) for the event. This also allows us to know what energy deposition is attributed to a given particle (e.g., the electrons) or track (a specific track within an event).
Position vectors, local and global	Where the track is located in the coordinate system of the local volume and of the world (global) volume.
Physics process ID	An integer associated with a physics process responsible for creating this track.
Weight	If physics bias is selected, the track is given a fractional weight. Otherwise it is set to 1. The inverse of the weight is the effective number of events that would have been required to generate the given event or track, had physics bias not been used. Using the weight value in the analysis is how the correct cross sections are restored. Biasing allows very significant speedup factors while generating the events. In the case of a 500-micron-thick diamond, the factor is about 100.

3.2 MCNP6.2 simulations

The same diamond detector geometry modeled in Geant4 was modeled in MCNP6.2 utilizing the ENDF/B-VII.1 cross-section library with the same material properties to provide cross-code validation. A 2-D representation of the MCNP6.2 diamond detector model is provided in Figure 4. In this case, the diamond was surrounded by air at standard temperature and pressure. A 14.1 MeV monoenergetic isotropic neutron source was placed 0.05 mm from one face of the diamond.

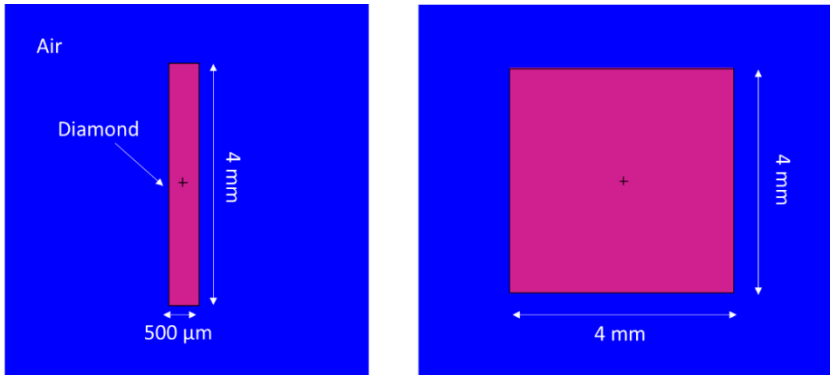

Figure 4. Two-dimensional representation of MCNP6.2 diamond detector model: side view (*left*) and front view (*right*).

Similar to the Geant4 model, elastically and inelastically scattered neutrons, gamma rays, electrons, alpha particles, protons, deuterons, and recoil ^{12}C and ^{13}C ions produced from the various 14.1 MeV neutron interactions in the diamond volume were tracked. The average flux and energy deposition for each of these radiation quanta were tallied as a function of energy and time. The F4 and F6 tallies in MCNP6.2 were used to calculate the average particle flux over the diamond cell (particles/cm^2/source particle) and the average energy deposition in the diamond cell (MeV/g/source particle), respectively. The results of the F6 tally were multiplied by the mass of the diamond (g) to obtain units of MeV/source particle. These outputs were utilized for cross-code validation by comparison to the Geant4 results.

4. ANALYSIS AND RESULTS

4.1 Geant4 results

We generated event samples of neutrons at 14.1 MeV initially to study the effects that the primary D-T neutrons would have on the diamond detector. It became clear that we would also need to run a full energy spectrum up to slightly past the ideal energy of neutrons emitted from D-T fusion. Since neutron detection is of primary interest here, we also generated a similar set of gamma spectra over the same energy range so that we can develop strategies for neutron and gamma discrimination and for building better detectors out of this medium. The plots in these studies are made from this simulation's output ntuple (Table 1), which contains all of the information required to not only plot the variables of interest, but also correlate or select the particles or events fulfilling a given requirement.

4.1.1 Neutrons at 14.1 MeV

This survey of the physics of D-T neutrons on diamond comes from a run of 1E8 monoenergetic neutrons, which was done in "analog" (to borrow a term from the MCNP literature) with no cross-section biasing. This resulted in about 1.1E6 events in which a neutron interaction occurred. We have made a number of distributions from this set, which tells us about the rich dynamics of particles and interactions that may occur in reality. Figure 5 exhibits the various particle types that are encountered, with its bottom plot showing the occurrence of alpha particles, beryllium, and carbon isotopes as roughly expected by their relative cross sections and abundances. The expected values differ somewhat from what the simulation shows possibly due to the current limitation of the use of the aggregate natural carbon cross sections, whether the neutron encounters a simulated ^{12}C or ^{13}C in the material. We hope to delve further into these questions at a later time.

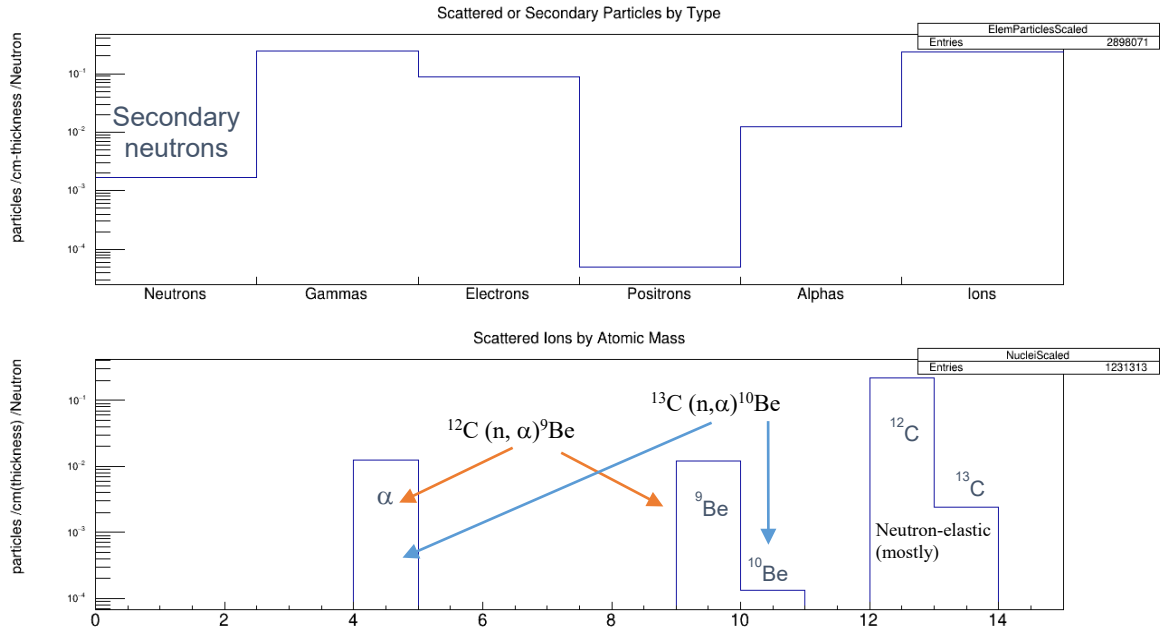

Figure 5. The distribution of the types of particle either created or scattered by the incoming neutron.

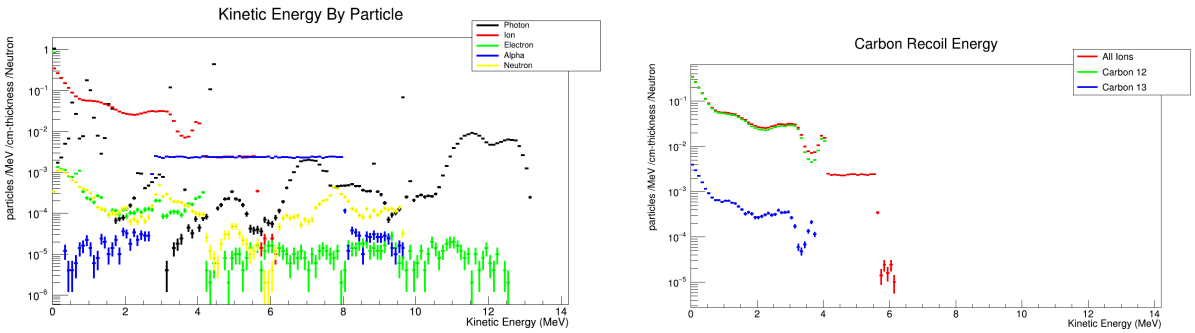

Figure 6. The distributions of kinetic energies of particle tracks by particle type. Note the dominance of ions. Though photons are also present here, they result in very little contribution to the energy deposition relative to the ions and alphas. The plot on the right shows the ^{12}C and ^{13}C in comparison to all heavy ions.

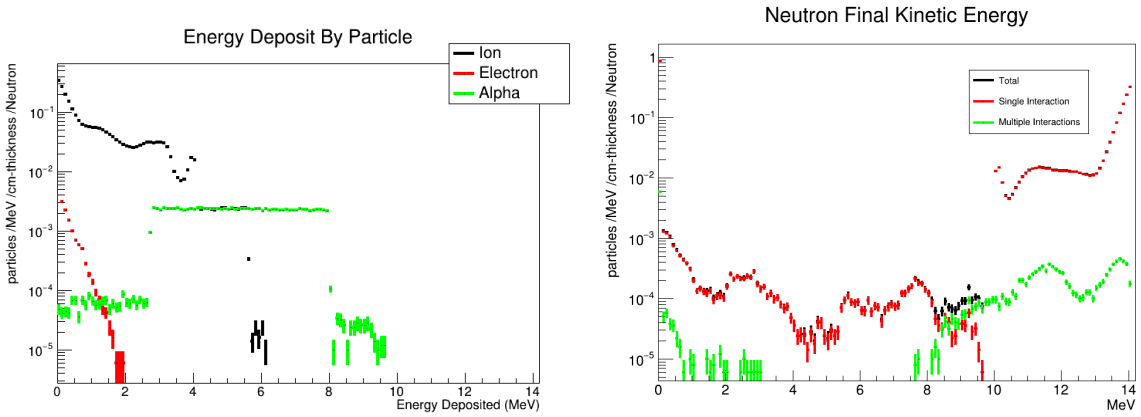

Figure 7. The energy deposition is ultimately what creates the signal. This shows the relative contributions from displaced ions, alpha particles, and electrons. On the right, the final kinetic energies of the neutrons are plotted with emphasis on showing whether the neutron encountered multiple interactions in the event.

The above distributions show that the energy deposition occurs mostly from displaced carbon nuclei resulting from elastic interactions with the beam neutron. The ions, such as ^{9}Be and ^{10}Be (and correlated alphas), resulting from inelastic interactions contribute, but far less than displaced ^{12}C and ^{13}C ions. The vast majority are single interactions with neutrons in which the neutron gives ~1–4 MeV to a carbon atom through elastic scattering.

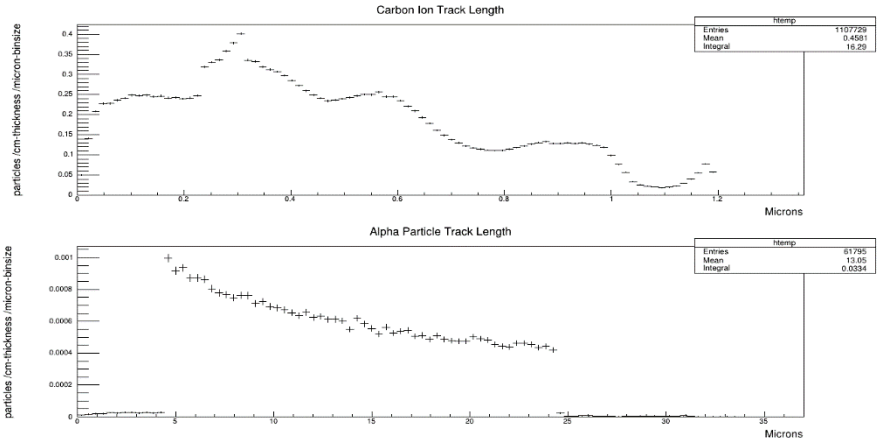

Figure 8. Carbon ion and alpha particle track length histograms.

A study of the tracking distributions is also interesting. As seen in Figure 8, we looked at the lengths of particle tracks if they were ions, alphas, and (later in this paper) electrons and positrons. While the alphas have a decade longer track length, they will still be well contained in a 500-micron slab. In Figure 9, we show the distribution of carbon ion position after being scattered by the beam neutron, which enters at the center of the diamond for our simulation. The lower plot shows that the distribution of ion position along the thickness of the diamond is entirely uniform. This follows from the fact that the interaction length of several centimeters is much longer than the thickness of the diamond slab.

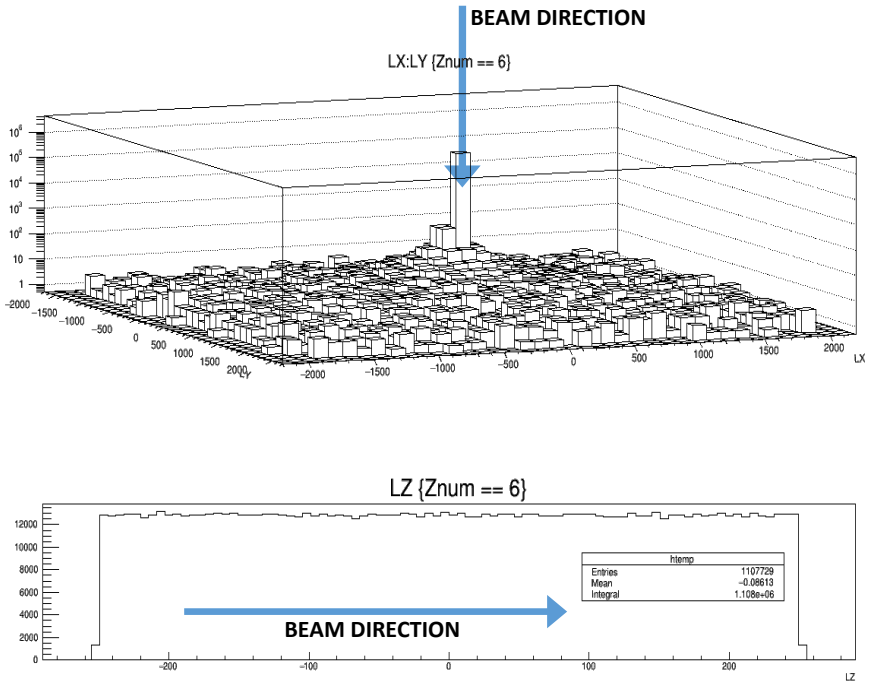

Figure 9. Histogram of scattered carbon ion position within the diamond slab. Dimensions are in microns. The bottom plot is along the thickness dimension, showing that the ion scattering runs uniformly along the thickness.

4.1.2 Neutrons and gammas from 10 KeV to 14.5 MeV

In this section, we study the full energy range expected of a realistic environment. Both neutrons and gammas are simulated from 10 KeV to 14.5 MeV, as seen in Figure 10.

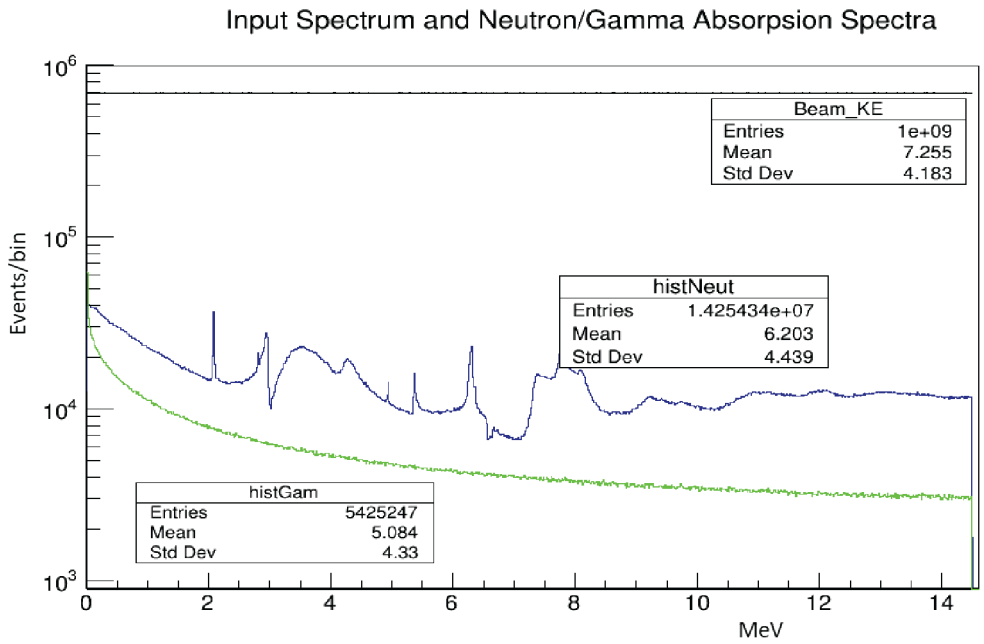

Figure 10. Histograms of beam energy. The top line is what was generated: a uniform distribution of 1E9 events over all energies for separate gamma and neutron runs. The blue and green are also beam kinetic energy histograms, but with the requirement that a neutron (*blue*) or gamma (*green*) event occurred. The selection bias effectively makes the bottom distributions absorption spectra of the beam particles.

For the 10 KeV to 14.5 MeV neutron run, Figures 11 and 12 are given. The 2-D histogram in Figure 11 shows the structure that we get when the energy deposition is correlated to the beam energy. One event constitutes one entry into the histogram, given that the event has $E_{dep} > 0$. The major structures in the plot show the Be + alpha events, the elastic scattering events, and ones in which particles left the diamond and did not stop (the various constant slopes going through the origin). It is notable in Figure 12 that the typical track lengths of the particles shown have very different length scales. The ions are the shortest, as expected, and leave their energy in <1 micron. The alphas do this in tens of microns, and the electrons do this in hundreds of microns or more and are the most likely to leave the volume. The difference especially between the ions and electrons can be a helpful discriminator as is discussed later.

For the gamma run over the same energy range, we have Figures 13 and 14. These indicate a very different set of particles created and energy-loss mechanism. Electrons, positrons, and gammas are the only particles seen in this simulation. Similar to Figure 11, Figure 13 shows the 2-D histogram of E_{dep} vs. gamma beam energy. As noted above, the energy deposition is over a longer range and is fully electromagnetic. There are much fewer discrete reaction types at this energy range; hence, this data sample has much less structure than that of the neutron beam simulation data.

In terms of track length and energy loss, showing a plot of ion kinetic energy is nearly identical to showing a plot of ion energy loss. The typical track length of ions in diamond is a little less than 1 micron. In contrast, alpha track length is an order of magnitude higher, and electrons higher still. This implies that beam gammas at these energy scales, which are mostly Compton scattering and pair producing with the medium, will inherently have lower energy loss per unit thickness of diamond as compared to neutron elastic events. In addition to the low gamma + carbon cross section, this "sifting effect" caused by the energy-loss differential should also help with the ubiquitous n/γ discrimination problem. This is promising, but a large flux of low-energy KeV photons will negatively impact signal-to-noise ratio. However, this could be mitigated by thin shielding, which will have relatively little effect on the neutrons.

Finally, in Figure 15, we show the mean E_{dep} response as a function of beam energy. Because it includes events in which $E_{dep} = 0.0$, a known spectrum of incoming gammas or neutrons can be directly translated into an energy deposition in the diamond detector without reference to cross sections. The E_{dep} would then be used to compute the detector signal based on its known electronic characteristics.

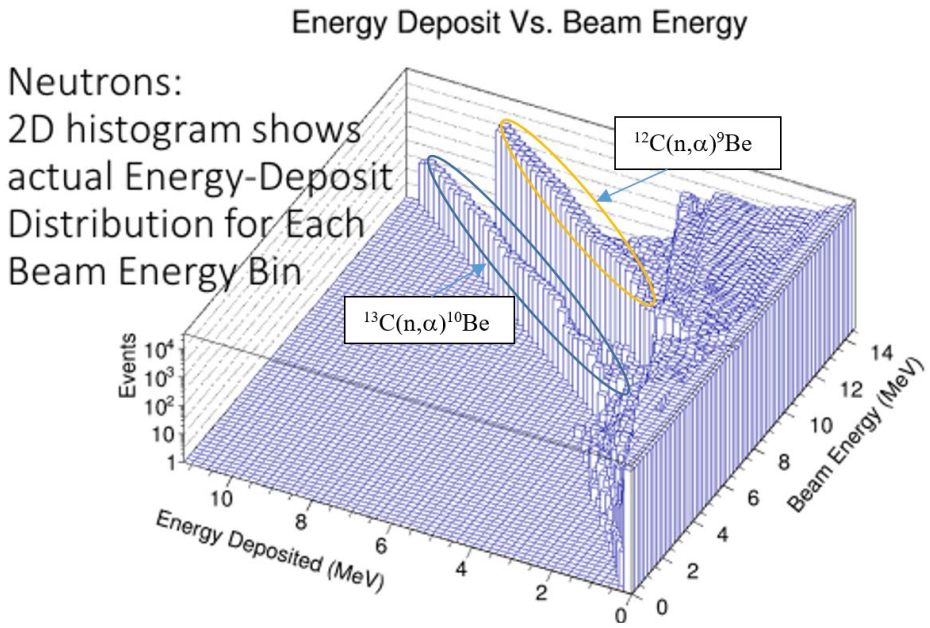

Figure 11. Two-dimensional histogram of the energy deposited per event vs. the neutron beam energy. One entry is made for every event in which E_{dep} is nonzero.

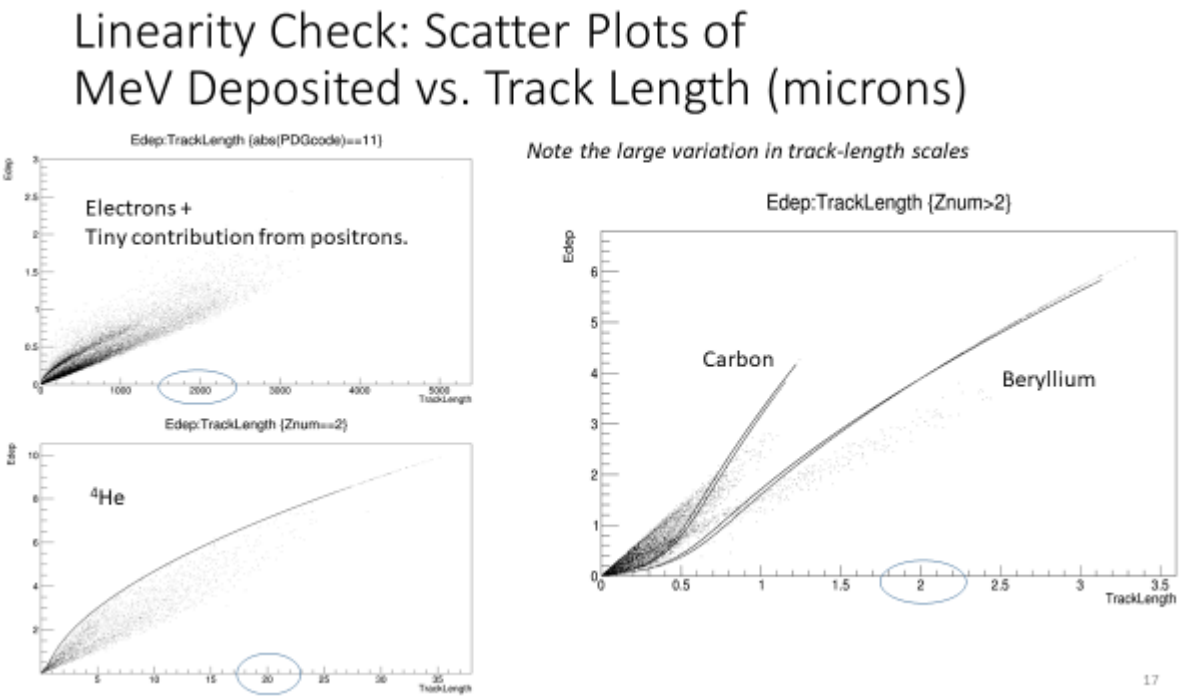

Figure 12. Two-dimensional scatter plots of energy deposited vs. the track length. One entry (dot) is made per particle of the specified type.

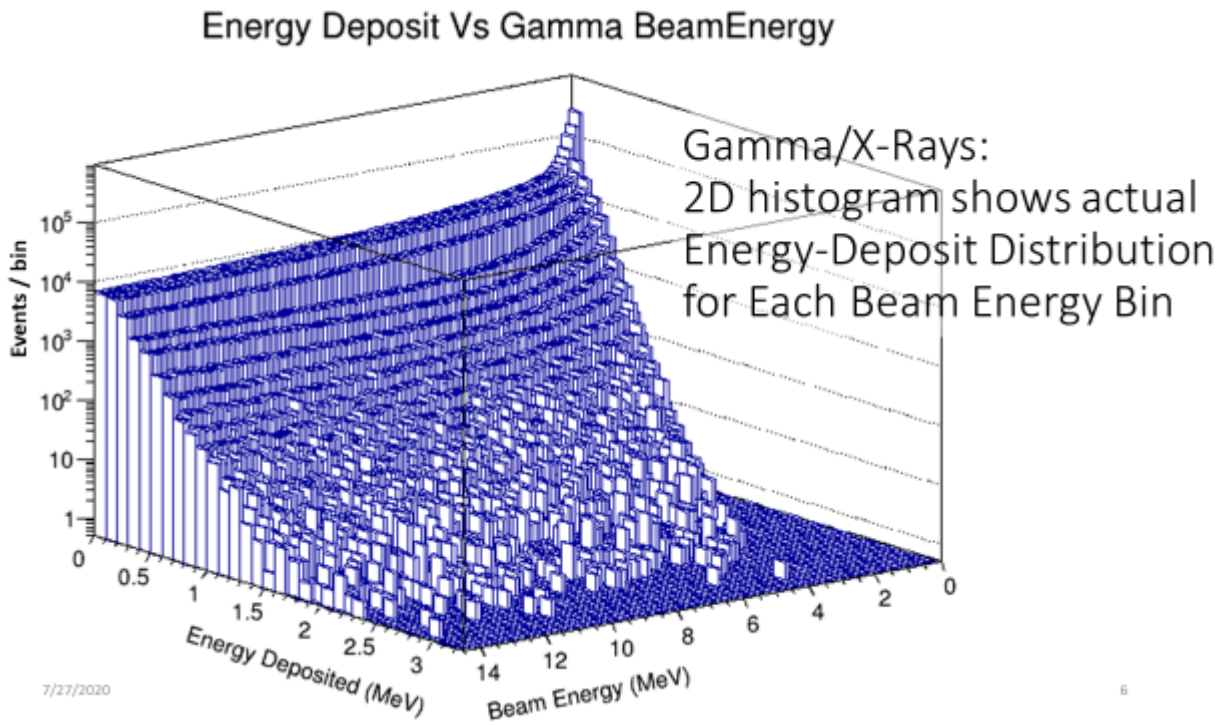

Figure 13. Two-dimensional histogram of the energy deposited per event vs. the gamma beam energy. One entry is made for every event in which E_{dep} is nonzero.

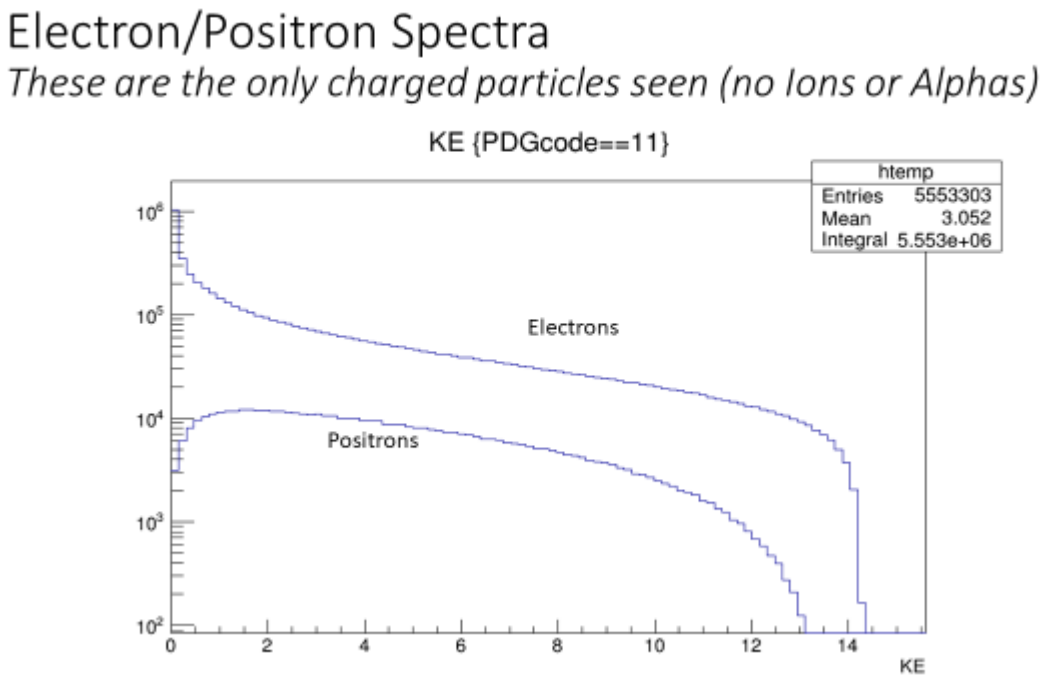

Figure 14. From gamma beam events over the 10 KeV to 14.5 MeV range. Electrons, positrons, and photons are the only particles seen in this 1E9-event sample.

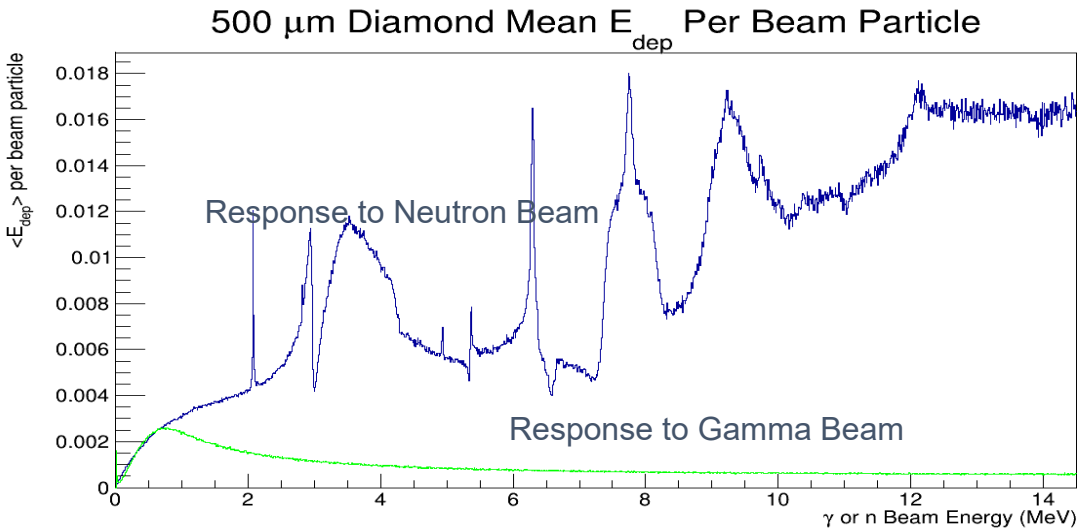

Figure 15. This is the energy deposition response function, which gives the mean MeV deposited as a function of beam energy. This includes whether or not the event has interactions, i.e., the mean E_{dep} includes the $E_{dep} = 0$ events. From this, a known spectrum of incoming gammas or neutrons can be directly translated into an energy deposition without reference to the cross sections.

4.2 MCNP6.2 results

4.2.1 Average neutron flux

The first indication of the presence of neutrons and their possible interactions in the diamond from the MCNP6.2 simulations is provided by the results of the F4 tally. The F4 tally cell-averaged flux as a function of neutron energy in MeV is shown in Figure 16. It is discerned from Figure 16 that the majority of 14.1 MeV neutrons incident on the diamond do not lose any of their energy and pass right through the diamond volume. This makes sense because the diamond is so thin (only 500 μm) and the incident neutrons have a fairly high energy. The probability of a 14.1 MeV neutron making any interaction in the diamond is only ~1%. However, these interactions are evident in Figure 16 at energies below 14.1 MeV.

The cell-averaged flux between 10 MeV and 14.1 MeV in Figure 16 is representative of the distribution of elastically scattered 14.1 MeV neutrons. The maximum energy loss expected from an elastically scattered 14.1 MeV neutron on a ^{12}C atom is 4.00 MeV. This corresponds to a neutron with a final kinetic energy of 10.1 MeV. Similarly, the average energy loss is 2.00 MeV. This corresponds to a neutron with a final kinetic energy of 12.1 MeV. The cell-averaged flux shown in Figure 16 exhibits a peak at ~12 MeV and a drop-off at ~10 MeV. These features agree with the expected distribution of elastically scattered 14.1 MeV neutrons. The cell-averaged flux below 10 MeV can be attributed to a combination of inelastically scattered neutrons and neutrons being elastically scattered more than one time.

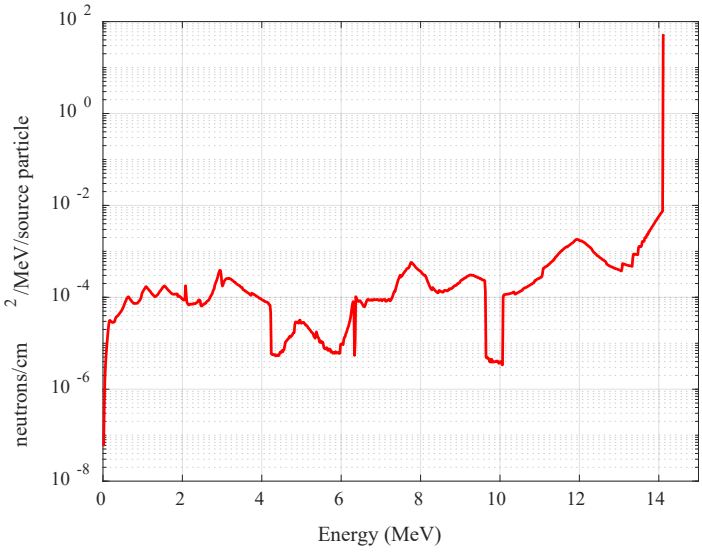

Figure 16. MCNP6.2-calculated average flux of neutrons in 4 × 4 × 0.5 mm^3 diamond.

4.2.2 Energy deposition

It is ascertained from Figure 17 that recoil carbon ions from elastically scattered neutrons deposit the most energy in the diamond and thus contribute the most to the measured signal. The recoil ion energy deposition represented by the red line in Figure 17 consists of contributions from both ^{12}C and ^{13}C recoil ions from elastically scattered neutrons. It is approximately three orders of magnitude higher than the energy deposition from charged particles created in the diamond from inelastic scattering interactions. These findings are consistent with those found from the Geant4 results.

Figure 18 breaks out the energy deposition from ^{12}C and ^{13}C recoil ions in to two separate lines, red and blue, respectively. The energy deposition from the ^{12}C recoil ions is approximately two orders of magnitude higher than the energy deposition from the ^{13}C recoil ions. This intuitively makes sense because the isotopic abundance of ^{12}C in the diamond is almost two orders of magnitude greater than that of the ^{13}C. This is also consistent the comparison of the ^{12}C and ^{13}C energy deposition found with Geant4.

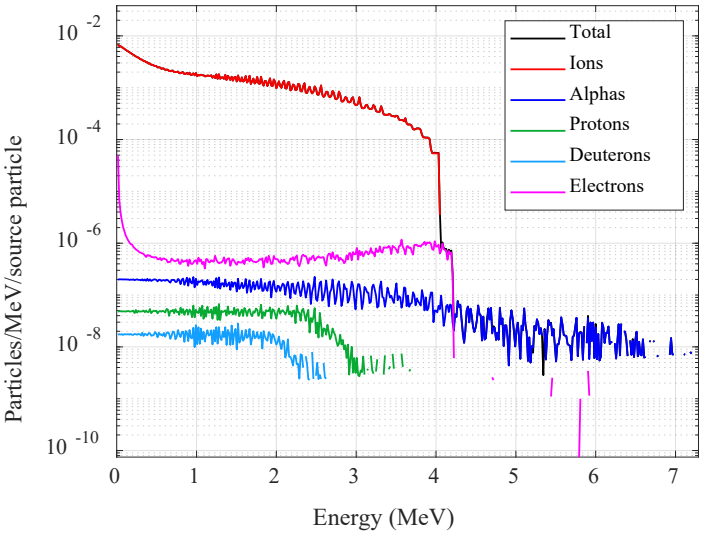

Figure 17. MCNP6.2-calculated energy deposition from all charged particles in 4 × 4 × 0.5 mm^3 diamond.

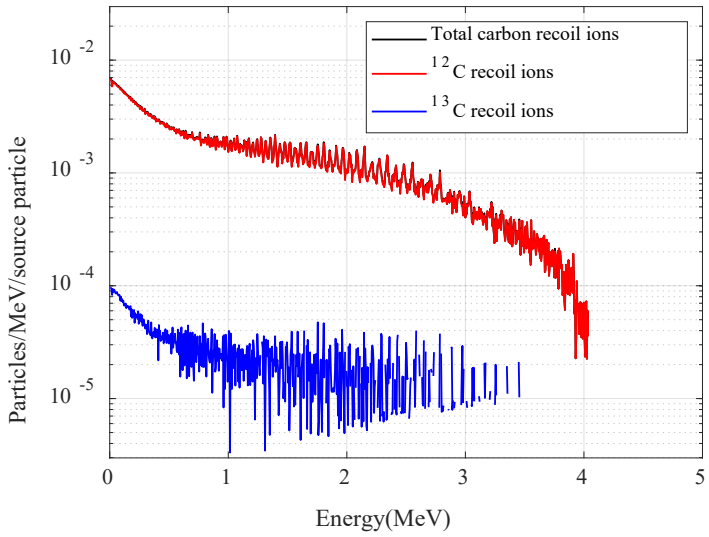

Figure 18. MCNP6.2-calculated energy deposition from carbon recoil ions in 4 × 4 × 0.5 mm^3 diamond.

4.3 Comparison of Geant4 and MCNP6.2 results

4.3.1 Calculation of macroscopic cross sections

One of the comparisons made was to look at the basic correspondence of the number of interactions of a given type per unit thickness of diamond. This is known as the "macroscopic" cross section. The elastic cross sections are the most important modes and also have reasonable correspondence. As previously stated, Geant4 reports in its output that it uses natural carbon cross sections instead of those of individual isotopes. This is understandable, but it will cause some discrepancies when a neutron interacts with a specific isotope as it must. In the end, due to the dominance of ion energy loss, the agreement of the totals ensures reasonable correspondence of energy-loss predictions.

Table 2. Comparison of macroscopic 14.1 MeV neutron + carbon cross sections (Σ) of elastic, inelastic, and total when applied to natural diamond with density of 3.51 g/cm^3.

Interaction with 14.1 MeV Neutrons	**Calculated Σ (cm^{-1})**	**MCNP Σ (cm^{-1})**	**Geant4 Σ (cm^{-1})**
^{12}C Elastic	1.37E-01	1.40E-01	1.44E-01
^{12}C Inelastic	9.32E-02	8.74E-02	8.41E-02
^{12}C Total	2.29E-01	2.28E-01	2.28E-01
^{12}C Elastic	1.49E-03	1.87E-03	1.20E-03
^{12}C Inelastic	1.28E-03	1.61E-03	1.29E-03
^{12}C Total	2.77E-03	3.12E-03	2.49E-03
Total	2.32E-01	2.31E-01	2.31E-01

5. CONCLUSIONS

We have simulated the effects of neutrons and gammas on scCVD diamonds for the purpose of eventual detector optimization for the potential use in NDSE campaigns. The MCNP and Geant4 results are consistent, though not entirely the same. More can be understood here. We have also used these simulations to better understand the energy-loss

mechanisms and relative importance of elastic scattering vs. other processes, as well as the relative contributions from ions, alphas, electrons, and others. This information will be used to further the detector design process.

ACKNOWLEDGMENTS

This manuscript has been authored by Mission Support and Test Services, LLC, under Contract No. DE-NA0003624 with the U.S. Department of Energy and supported by the Site-Directed Research and Development Program, NA-10 USDOE NA Office of Defense Programs (NA-10). The United States Government retains and the publisher, by accepting the article for publication, acknowledges that the United States Government retains a non-exclusive, paid-up, irrevocable, worldwide license to publish or reproduce the published form of this manuscript, or allow others to do so, for United States Government purposes. The U.S. Department of Energy will provide public access to these results of federally sponsored research in accordance with the DOE Public Access Plan (http://energy.gov/downloads/doe-public-access-plan). The views expressed in the article do not necessarily represent the views of the U.S. Department of Energy or the United States Government. DOE/NV/03624--0842.

REFERENCES

[1] Bäni, L., et al., "Diamond detectors for high energy physics experiments," J. Instrum. 13, CO1029 (2018).
[2] Williams, T. et al., "Operation of a fast diamond γ-ray detector at the HIγS facility," Nucl. Instrum. Methods Phys. Res. A 830, 391–396 (2016).
[3] Tong, X., Thompson, J., and Byun, S. H., "Development of a scCVD diamond detector as a transmission-type alpha particle counter," Nucl. Instrum. Methods Phys. Res. A 954, 161594 (2020).
[4] Knoll, G. F., [Radiation Detection and Measurements, Fourth Edition], John Wiley & Sons, Hoboken, NJ (2010).
[5] Dueñas, J. A., Mora, J. M., Traeger, M., Galbiati, A., Martel, I., and Berdermann, E., "Time response of 50 μm thickness single crystal diamond detectors," Diam. Relat. Mater. 55, 144–148 (2015).
[6] Skukan, N., Sudić, I., Pomorski, M., Kada, W., and Jakšić, M., "Enhanced radiation hardness and signal recovery in thin diamond detectors," AIP Adv. 9, 025027 (2019).
[7] Hatarik, R., Sayre, D. B., Caggiano, J. A., Phillips, T., Eckart, M. J., Bond, E. J., Cerjan, C., Grim, G. P., Hartouni, E. P., Knauer, J. P., Mcnaney, J. M., and Munro, D. H., "Analysis of the neutron time-of-flight spectra from inertial confinement fusion experiments," J. Appl. Phys. 118, 184502 (2015).
[8] Kabadi, N. V., Sio, H., Glebov, V., Gatu Johnson, M., MacPhee, A., Frenje, J. A., Li, C. K., Seguin, F., Petrasso, R., Forrest, C., Knauer, J., and Rinderknecht, H. G., "Sensitivity of chemical vapor deposition diamonds to DD and DT neutrons at OMEGA and the National Ignition Facility," Rev. Sci. Instrum. 87, 11D817 (2016).
[9] Jones, B., et al., "Neutron diagnostics on the Z machine," Sandia National Laboratories, SAND2014-17543PE (2014).
[10] "A demonstrated dense plasma focus NDSE diagnostic for Excalibur," Los Alamos National Laboratory and Mission Support and Test Services, LA-UR-18-26141 (2018).
[11] Allison, J., et al., "Recent developments in Geant4," Nucl. Instrum. Methods Phys. Res. A 835, 186–225 (2016).
[12] Werner, C. J., ed., "MCNP users manual: Code version 6.2," Los Alamos National Laboratory, LA-UR-17-29981 (2017).
[13] "Geant4, a simulation toolkit: Guide for physics lists," Release 10.5, Geant4 Collaboration, March 2019.
[14] Brun, R., and Rademakers, F., "ROOT—An object oriented data analysis framework," Nucl. Instrum. Methods Phys. Res. A 389(1–2), 81–86 (1997). See also http://root.cern.ch/.